HOVER PERFORMANCE PREDICTIONS OF COAXIAL ROTOR CONFIGURATIONS USING THE UPDATED CMTSVT MULTIROTOR INFLOW MODEL

Feyyaz Guner
feyyaz.guener@dlr.de
Institute of Flight Systems
German Aerospace Center (DLR)
Lilienthalplatz 7, D-38108, Braunschweig, GERMANY

Abstract

This paper uses the **c**ombined **m**omentum **t**heory and **s**imple **v**ortex **t**heory (CMTSVT) multirotor inflow model for hover performance predictions of coaxial rotor configurations. The CMTSVT inflow model is updated with the wake contraction and decay functions, and their effects on performance predictions are discussed. For comparison, wind tunnel measurements available in the literature are used to study the effects of loading changes at the fixed axial separation distance and different axial separation distances at fixed loading settings. Apart from the figure of merit, power, and thrust sharing ratio predictions, factors such as the interference loss and rotor-rotor influence loss are determined to identify rotor-rotor interaction effects on the performance. Furthermore, the total, self, interference uniform inflow components along with the lower rotor inflow distributions plots are provided for further insight. It has been shown that additions of the wake contraction and decay functions tremendously improve the predictions of the CMTSVT inflow model. With additions of these real-flow effects, the CMTSVT inflow model can capture the effects of rotor-rotor interactions for different loading settings and axial separation distances.

NOMENCLATURE

Symbols

C_L	aerodynamic roll moment coefficient	
C_M	aerodynamic pitch moment coefficient	
C_P	total power coefficient	
C_{P_i}	induced power coefficient	
C_Q	torque coefficient	
C_T	aerodynamic thrust coefficient	
D	rotor diameter	m
FM	figure of merit	
N_b	number of blades	
N_R	number of rotors	
V_T	nondimensional total flow passing through rotor	
$\bar{r}$	nondimensional radial blade coordinate	
z	axial separation distance	m

Greek Symbols

χ	wake skew angle	rad
κ_{int}	interference loss factor	
κ_u, κ_l	rotor-rotor influence loss factors	
λ_0	uniform inflow component	
λ_{1c}	longitudinal inflow component	
λ_{1s}	lateral inflow component	
μ	advance ratio	
μ_f	advance ratio component parallel to inflow	
ψ	azimuth angle	rad
$\bar{\psi}$	wake azimuth angle	rad

θ_{twst}	linear blade twist	$^\circ$

Superscripts

j	rotor index
S, I	show relation to the self and interference inflow components, respectively

Subscripts

c, s	show relation to the coaxial rotor and the single rotor, respectively
u, l	show relation to the upper rotor and the lower rotor, respectively

1. INTRODUCTION

Current interest in Urban Air Mobility (UAM) and Advanced Air Mobility (AAM) markets has led to the development of new vertical lift vehicles with multiple lifting rotors. The latest press release of the Vertical Flight Society [1] revealed that more than 600 multirotor vehicle concepts with different rotor arrangements and sizes are proposed. The vast majority of these multirotor vehicles are subject to rotor-rotor inflow interactions in one form or another since they operate within a complex flow field unique to the proposed configuration. Some vehicles might be subject to more interaction in hover, while others might suffer more from the interaction effects in the transition phase of the flight. It is crucial to predict the rotor-rotor interaction effects as early as possible in the design and optimization of vehicle aerodynamic performance and other aspects such as flight simulations and handling qualities analyses.

To capture rotor-rotor interaction effects and predict flow fields of generic multirotor configurations, high or mid-fidelity wake models based on computational fluid dynamics (CFD) [2, 3], free-vortex wake [4–10], viscous vortex particle method (VVPM) [11], and hybrid modeling approaches [12] are frequently used. It is also possible to use models with relatively lower fidelity based on potential flow theory and rigid wake formulation. These models employ the superposition approach to arrive at analytical finite-state multirotor inflow models, such as the **p**ressure **p**otential **s**uperposition **i**nflow **m**odel (PPSIM) [13] and the **v**elocity **p**otential **s**uperposition **i**nflow **m**odel (VPSIM) [14]. These models have previously been shown to capture fundamental rotor-rotor interaction effects among the rotors. Guner and Prasad [15] proposed a simpler model known as the **c**ombined **m**omentum **t**heory and **s**imple **v**ortex **t**heory (CMTSVT) multirotor inflow model by combining the extended momentum theory inflow model with a rigid vortex wake theory. The CMTSVT inflow model is one of the simplest inflow models considering the rotor-rotor interaction effects of generic multirotor configurations. References 15–17 have shown some validation cases by comparing the CMTSVT inflow model with experimental data and other multirotor inflow models for various configurations. More recently, the CMTSVT inflow model has been reformulated into a state-space form, which has made the time marching simulations possible [18].

Although the CMTSVT inflow model has previously been compared against other inflow models and some experimental data [15–17], the model has not been validated in detail for different configuration parameters. In particular, rotor-rotor interaction effects for varying axial separation distances in coaxial rotor configurations are not studied. Ramasamy conducted a series of hover experiments to determine the performance of coaxial rotor configurations [19]. He provided the figure of merit and power measurements concerning varying thrust settings for a given coaxial rotor configuration at a fixed axial separation distance. Besides, he varied the axial separation distance between the rotors while maintaining the total thrust of the system to analyze the effects of rotor-rotor interactions in the coaxial rotor performance predictions. Furthermore, Ramasamy [19] provided induced power interference loss factors (κ_{int}), load sharing ratios (T_l/T_u), and rotor-rotor influence loss factors (κ_u, κ_l) with respect to the axial separation distance. Reference 20 has used an iterative blade element momentum theory model and shown that analytical models can capture general trends in coaxial rotors' performance predictions using Ref.19. Other analytical models employ simple corrections to momentum theory-based models for capturing some of the rotor-rotor interaction effects in dual-rotor configurations [21, 22].

Despite the encouraging results of simple modeling approaches [20–22], their applications are limited to some instances and cannot be used as a generalized tool. On the other hand, the CMTSVT inflow model is a generic multirotor inflow model that can be applied to any configuration, that is, coaxial, tandem, or quad-rotor. It is a versatile model that can be used in performance predictions, design trade-off studies, flight simulations, and handling qualities analyses. However, the model is based on potential flow theory and does not consider real-flow effects such as wake contraction and wake decay. This paper introduces analytical wake contraction and

wake decay functions to the CMTSVT inflow model. Along with the original formulation, these effects are systematically studied and compared against the data set provided in Ref. 19. The total, self, interference uniform inflow components, and inflow distributions for various axial separation distances are also provided to gain further insight.

The paper is organized as follows: first, the formulation of the CMTSVT inflow model is summarized. Then, analytical wake contraction and wake decay functions are introduced. After that, a few single rotor performance predictions are provided to determine some of the rotor blade parameters. These are followed by coaxial rotor performance predictions and rotor-rotor interaction analyses. The wake contraction function, uniform inflow components, and lower rotor inflow distributions as a function of axial separation distance are also provided for additional discussion. Finally, significant outcomes are summarized, and recommendations are given.

2. COMBINED MOMENTUM THEORY AND SIMPLE VORTEX THEORY INFLOW MODEL

The CMTSVT inflow model is formulated by combining the extended momentum theory inflow model with a simple vortex theory [15]. This model takes advantage of the simplicity of the momentum theory and a rigid wake vortex theory to arrive at a model that includes fundamental rotor-rotor interaction effects.

In the CMTSVT inflow model, the total inflow on a rotor is described as the summation of self-induced inflow (λ^S) and interference inflow (λ^I) components due to other rotors, i.e., $\lambda(\bar{r},\bar{\psi}) = \lambda^S(\bar{r},\bar{\psi}) + \lambda^I(\bar{r},\bar{\psi})$. After approximating the inflow distribution with the first harmonic inflow expansion, the inflow distribution of the *jth* rotor is expressed as:

$$\lambda^j(\bar{r},\bar{\psi}) = (\lambda_0^{j,S} + \lambda_0^{j,I}) + (\lambda_{1c}^{j,S} + \lambda_{1c}^{j,I})\bar{r}\cos\bar{\psi} + (\lambda_{1s}^{j,S} + \lambda_{1s}^{j,I})\bar{r}\sin\bar{\psi} \quad (1)$$

In Eq. (1), the superscript *j* refers to the rotor index. Unlike the single rotor configurations, the total flow passing through each rotor must be modified to account for interference inflow components, which provide additional air mass to each rotor. This additional air mass also affects the magnitude of the self-induced inflow. The self-induced uniform inflow of the *jth* rotor is calculated by Eq. (2).

$$\lambda_0^{j,S} = C_T^j/(2V_T^j) \quad (2)$$

where

$$V_T^j = \sqrt{(\mu^j)^2 + (\mu_f^j + \lambda_0^j)^2}$$

$$\lambda_0^j = \lambda_0^{j,S} + \lambda_0^{j,I}$$

An iterative process is required to solve for the self-induced uniform inflow component of each rotor (λ_0^S) until all self-induced and interference uniform inflow components converge. Once they converge, the first harmonic inflow components of the *jth* rotor are obtained from the modified dynamic inflow formula of Pitt and Peters as follows [23]:

$$\lambda_{1c}^j = \lambda_{1c}^{j,S} + \lambda_{1c}^{j,I} \quad (3)$$

$$\lambda_{1s}^j = \lambda_{1s}^{j,S} + \lambda_{1s}^{j,I} \quad (4)$$

where

$$\lambda_{1c}^{j,S} = \frac{15\pi}{64V_T^j}\tan\frac{\chi^j}{2}C_T^j - \frac{4\cos\chi^j}{V^j(1+\cos\chi^j)}C_M^j$$

$$\lambda_{1s}^{j,S} = -\frac{4}{V^j(1+\cos\chi^j)}C_L^j$$

$$V^j = \frac{(\mu^j)^2 + (\mu_f^j + \lambda_0^j)(\mu_f^j + 2\lambda_0^j)}{V_T^j}$$

$$\chi^j = \tan^{-1}\frac{\mu^j}{\mu_f^j + \lambda_0^j}$$

The interference uniform and first harmonic inflow components ($\lambda_0^{j,I},\ \lambda_{1c}^{j,I},\ \lambda_{1s}^{j,I}$) of the *jth* rotor are extracted from the interference inflow distribution. This interference inflow distribution is obtained from a rigid vortex theory based on simplified Biot–Savart law, formulated by Heyson [24]. Using Heyson's formula, interference inflow is calculated as:

$$\lambda^I(\bar{r},\bar{\psi}) = -\frac{1}{4\pi}\int_0^{2\pi} F(\psi)\Upsilon(\bar{x},\bar{y},\bar{z},\chi,\psi)\,d\psi \quad (5)$$

where

$$F(\psi) = \gamma_0 + \gamma_{1c}\cos\psi + \gamma_{1s}\sin\psi$$

$$\Upsilon = \frac{1 - (\bar{x}\cos\psi + \bar{y}\sin\psi) + R_c\sin\chi\cos\psi}{[R_c + (\cos\psi - \bar{x})\sin\chi + \bar{z}\cos\chi]R_c}$$

$$R_c = \sqrt{1 + \bar{x}^2 + \bar{y}^2 + \bar{z}^2 - 2(\bar{x}\cos\psi + \bar{y}\sin\psi)}$$

In Eq. (5), $\bar{x}$ and $\bar{y}$ represent Cartesian coordinates normalized by rotor radius (R) corresponding to an

aerodynamic calculation point in polar coordinates ($\bar{r}$ and $\bar{\psi}$). The vorticity variation around the azimuth is described as $F(\psi)$. Here, uniform (γ_0), cosine (γ_{1c}) and sine (γ_{1s}) parts of the vorticity are related to C_T, C_M, and C_L using the following equations [23].

$$\gamma_0 = \frac{C_T}{V_T(1-1.5\mu^2)} + \frac{3\mu C_L}{V_T(1-1.5\mu^2)} \quad (6)$$

$$\gamma_{1c} = -\frac{3C_M}{V_T} \quad (7)$$

$$\gamma_{1s} = -\frac{1.5\mu C_T}{V_T(1-1.5\mu^2)} - \frac{3C_L}{V_T(1-1.5\mu^2)} \quad (8)$$

After finding the interference inflow distribution at a rotor, the interference uniform, longitudinal and lateral inflow components are approximated using Eqs. (9), (10), and (11).

$$\lambda_0^I = \frac{1}{\pi}\int_0^{2\pi}\int_0^1 \lambda^I(\bar{r},\bar{\psi})\bar{r}\,d\bar{r}\,d\bar{\psi} \quad (9)$$

$$\lambda_{1c}^I = \frac{4}{\pi}\int_0^{2\pi}\int_0^1 \lambda^I(\bar{r},\bar{\psi})\bar{r}^2\cos\bar{\psi}\,d\bar{r}\,d\bar{\psi} \quad (10)$$

$$\lambda_{1s}^I = \frac{4}{\pi}\int_0^{2\pi}\int_0^1 \lambda^I(\bar{r},\bar{\psi})\bar{r}^2\sin\bar{\psi}\,d\bar{r}\,d\bar{\psi} \quad (11)$$

To obtain the total interference inflow at each of the individual rotors, interference inflow calculations are repeated for $(N_R-1)\times N_R$ times for a multirotor configuration with N_R being the number of rotors. In Eq. (12), indexing is provided for the *jth* rotor.

$$\{\lambda_0^{j,I},\ \lambda_{1c}^{j,I},\ \lambda_{1s}^{j,I}\} = \sum_{k=1,\ k\neq j}^{N_R}\{\lambda_0^{k,I},\ \lambda_{1c}^{k,I},\ \lambda_{1s}^{k,I}\} \quad (12)$$

2.1. Wake Contraction and Exponential Wake Decay Additions

The CMTSVT multirotor inflow model is based on the potential flow theory and rigid wake formulation. Like the PPSIM and VPSIM, it does not account for the contraction and decay of the wake. For the lower rotor of a coaxial rotor configuration, the wake contraction is significant as the lower rotor operates directly within the wake of the upper rotor in hover. If it is ignored, then the tip regions of the lower rotor blades receive higher wake velocities from the upper rotor instead of upwash or downwash close to zero. In addition to the wake contraction, a simple exponential wake decay function is introduced to the CMTSVT inflow model to account for some of the missing air viscosity effects. Reference 25 added these real-flow effects into the Peters-He finite state dynamic wake model and showed improved interference inflow predictions.

The wake contraction geometry can be obtained from flow field measurements or higher-order wake models for the selected configuration. Landgrebe [26] wake geometry functions, derived from the measurements of a rotor wake in isolation, are preferred instead of configuration-specific functions. The idea here is to capture the wake contraction effects somewhat while keeping the basic model approach and its generality. Landgrebe provided the following equation for the radial location of the tip vortex ($\bar{r}_{tip}$), which is normalized by the rotor radius.

$$\bar{r}_{tip} = 0.78 + (1-0.78)e^{-\Lambda\phi_w} \quad (13)$$

Here, ϕ_w is the wake age, and $\Lambda = 0.145 + 27C_T$. The wake age is obtained from the normalized axial location of the tip vortex ($\bar{z}_{tip}$) by equating it to normalized axial separation distance ($\bar{z} = z/R$) between the rotors. Landgrebe [26] provided the following formula for the axial location of the tip vortex:

$$\bar{z}_{tip} = \begin{cases} k_1\phi_w & \text{if } 0 \le \phi_w \le \frac{2\pi}{N_b} \\ \bar{z}_{tip_{\phi w = 2\pi/N_b}} + k_2(\phi_w - \frac{2\pi}{N_b}) & \text{if } \phi_w \ge \frac{2\pi}{N_b} \end{cases} \quad (14)$$

where

$$k_1 = 0.25\left(\frac{C_T}{\sigma} + 0.001\,\theta_{twst}\right)$$

$$k_2 = (1.41 + 0.0141\,\theta_{twst})\sqrt{C_T/2}$$

Since $\bar{z}_{tip}$ is taken equal to the axial separation distance between rotors ($\bar{z}$), one can solve for the ϕ_w using Eq. (15).

$$\phi_w = \begin{cases} \frac{\bar{z}_{tip}}{k_1} & \text{if } 0 \le \phi_w \le \frac{2\pi}{N_b} \\ \frac{\bar{z}_{tip}}{k_2} + \left(1 - \frac{k_1}{k_2}\right)\frac{2\pi}{N_b} & \text{if } \phi_w \ge \frac{2\pi}{N_b} \end{cases} \quad (15)$$

Once ϕ_w is obtained, it is straightforward to get the normalized radial location of the tip vortex ($\bar{r}_{tip}$) using Eq. (13). The $\bar{r}_{tip}$ modifies the radial coordinates

of the blade by dividing it into the nondimensional radial coordinate of the blade, i.e., $\tilde{r} = \bar{r}/\bar{r}_{tip}$.

Similar to the approach followed in Ref. 25, the wake decay effect due to air viscosity is modeled as a simple exponential function, that is, $w_d = e^{-\eta z/D}$. In this study, the wake decay coefficient (η) is taken as 0.2, and w_d is multiplied with $\lambda^I(\tilde{r}, \bar{\psi})$ for the inclusion of the decay effect in interference inflow distribution. It should be noted that the wake contraction and wake decay effects are only applied to the upper rotor downwash received by the lower rotor.

3. RESULTS AND DISCUSSIONS

The CMTSVT inflow model can predict rotor performance using the blade element and momentum theory relations frequently used to predict the induced, profile, and parasite power components of conventional main/tail rotor configurations. These relations can also predict the performance of multirotor configurations, given that the uniform inflow component of each rotor includes rotor-rotor inflow interactions. Then, the power (or torque) coefficient in hover can be estimated as [15]

$$(16)\quad C_P = C_Q = \sum_{j=1}^{N_R} \kappa C_T^j \lambda_0^j + \frac{\sigma^j}{8} C_d^j$$

where N_R is the number of rotors, the superscript j is the rotor index, κ is the induced power loss factor, and $C_d = \delta_0 + \delta_2 \alpha_m^2$. The zero drag coefficient is δ_0, whereas the quadratic part of the drag coefficient is described by δ_2. The term σ describes the solidity of each rotor, a_0 is the lift curve slope, and α_m is the mean blade angle, which is calculated by $6C_T/(a_0\sigma)$. Table 1 shows values used in the performance predictions of single and coaxial rotor configurations with untwisted blades at two different rotational speeds.

Table 1: Untwisted Rotor Blade Parameters.

Parameters	800 RPM Case	1200 RPM Case
N_b	3	3
κ	1.16	1.16
σ	0.0936	0.0936
δ_0	0.0123	0.0114
δ_2	0.9	0.7
a_0	5.73	5.73
θ_{twst}	0 °	0 °
D	1.32 m	1.32 m

In this study, experimental measurements are taken from Ref. 19, and these experimental values are simply referred to as ***data*** throughout the paper. Figure 1 shows the power predictions of 3-bladed ($N_b = 3$) and 6-bladed ($N_b = 6$) rotors in isolation at various thrust settings. The corresponding hovering efficiency (figure of merit) curves are provided in Fig. 2. The zero drag coefficient (δ_0) is determined from the data at the zero-thrust setting. The induced power loss factor (κ) and quadratic part of the drag coefficient (δ_2) are adjusted to fit reasonably with the data shown in Figs. 1 and 2. No attempt has been made to fine-tune these values. The same values are also used in all coaxial rotor configuration cases. This study focuses on capturing the performance trends of coaxial rotor configurations with either varying thrust settings or axial separation distances while keeping the other constant. It is always possible to fine-tune some parameters to

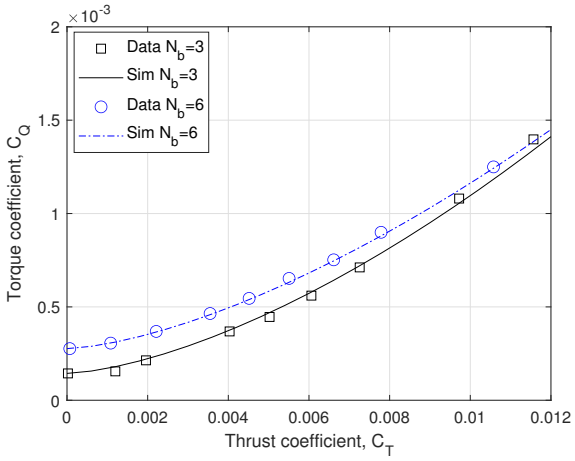

Figure 1: Single Rotor Torque Predictions at Various Thrust Settings ($RPM = 800$).

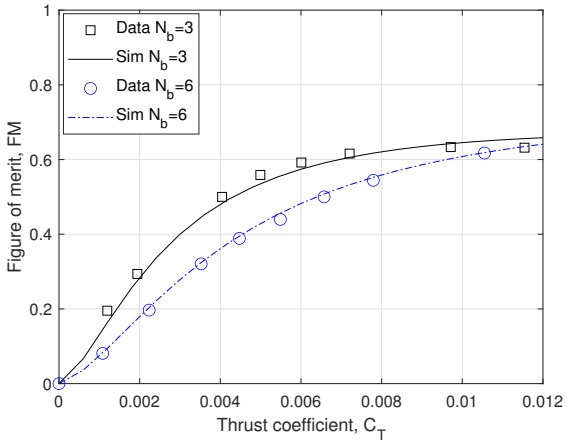

Figure 2: Single Rotor Figure of Merit Predictions at Various Thrust Settings ($RPM = 800$).

achieve better correlations. Nevertheless, δ_0 and δ_2 should have different values depending on the rotational speed of the rotor as it directly changes the Reynolds number that affects drag coefficients.

During his experiments, Ramasamy [19] trimmed the coaxial rotor configurations by balancing the rotor torque, i.e., $Q_u + Q_l = 0$. He either varied the total thrust of the system ($C_{T_c} = C_{T_u} + C_{T_l}$) at a fixed axial separation distance (z/D) or fixed the total system thrust to a selected value while varying the axial separation distance. This study follows the same method, and coaxial rotor simulations are always trimmed by balancing the torque. The simulation predictions are labeled throughout the paper as follows: *CMTSVT* refers to the original theory without the wake contraction and decay effects. *CMTSVT+WC* represents the model with wake contraction, while *CMTSVT+WC+WD* represents the model with both wake contraction and decay additions.

3.1. Loading Setting Sweeps at Fixed Axial Separation Distance

Performance measurements of a coaxial rotor configuration with the axial separation distance of $0.07D$ are provided in Fig. 3. As seen, the CMTSVT inflow model and its updated versions with only the wake contraction and both the wake contraction and the wake decay have better correlations with the data than the case without rotor-rotor interaction. At this separation distance, the wake contraction has a little effect on the predictions. By the same token, the wake decay effect is too small since the rotors are reasonably close to each other.

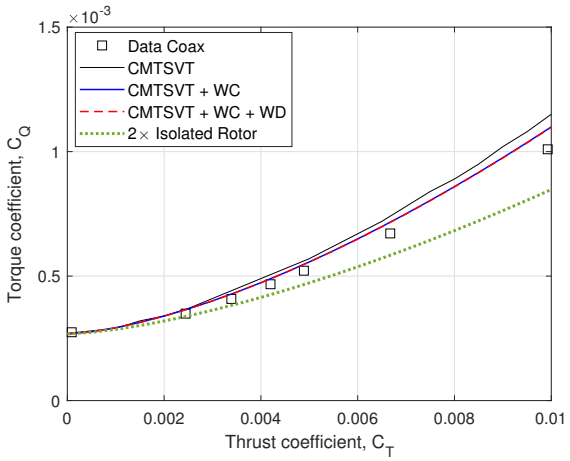

Figure 3: Performance Predictions of the Coaxial Rotor System at Various Thrust Settings ($RPM = 1200$, $z/D = 0.07$).

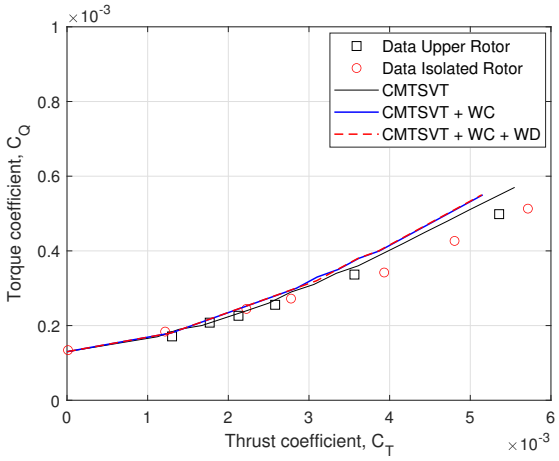

Figure 4: Performance Predictions of the Upper Rotor at Various Thrust Settings ($RPM = 1200$, $z/D = 0.07$).

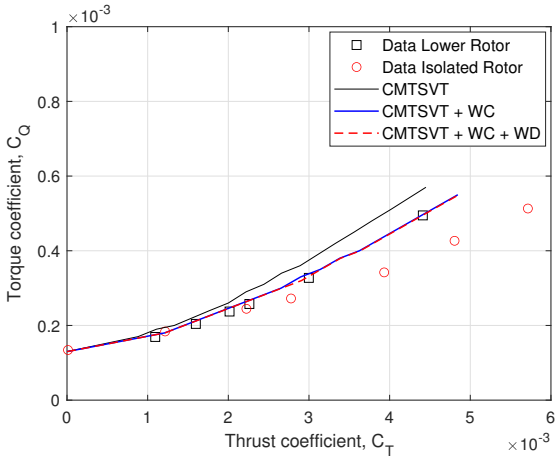

Figure 5: Performance Predictions of the Lower Rotor at Various Thrust Settings ($RPM = 1200$, $z/D = 0.07$).

Figures 4 and 5 illustrate the performance predictions of the upper and lower rotors, respectively, for the same coaxial rotor configuration. At the upper rotor, isolated and coaxial rotor data correlate well. At the same time, they are closely followed by the CMTSVT inflow model, especially at the lower thrust conditions. Surprisingly, the wake contraction addition slightly degrades the upper rotor torque prediction (Fig. 4). This deterioration might be due to the thrust sharing ratio change, which is explained in the next section. In contrast, the wake contraction addition significantly improved the lower rotor torque prediction (Fig. 5). The effects of inflow interaction in power predictions become apparent with increasing thrust settings. In this case, isolated rotor

torque measurements are less than the lower rotor torque measurements due to missing interaction effects indicating the importance of the rotor-rotor interactions in performance predictions.

3.2. Axial Separation Distance Sweep at Fixed Loading Setting

Figure 6 shows figure of merit predictions at thrust coefficients of 0.007 and 0.014 as a function of axial separation distance. The figure of merit of the coaxial rotor system is calculated as

$$FM = \frac{C_{T_u}^{3/2} + C_{T_l}^{3/2}}{\sqrt{2}(C_{Q_u} + C_{Q_l})} \quad (17)$$

It should be noted that thrust coefficients of individual rotors are used in the calculation of the figure of merit instead of the total coaxial rotor thrust coefficient. Detailed discussion on this selection is available in Refs. 19 and 21. In both thrust setting cases, predictions of the CMTSVT inflow model with the wake contraction and wake decay show a better correlation with the measurements of the coaxial rotor systems. Predictions are significantly improved compared to the original CMTSVT inflow model without any real-flow effect additions. At smaller axial separation distances ($z \leq 0.5D$), the wake decay effect is small as expected. The CMTSVT+WC+WD inflow model agrees well with the case only having the wake contraction effect, viz., CMTSVT+WC.

CMTSVT+WC and CMTSVT+WC+WD inflow models figure of merit predictions correlate even better at the lower rotor than the overall coaxial rotor system figure of merit predictions. The CMTSVT+WC+WD model predictions improve with the axial separation distance as the decay effect grows considerably. On the other hand, ignoring the real-flow effects, especially the wake contraction, result in pessimistic performance predictions at the lower rotor. This is because the entire lower rotor disk area receives downwash from the upper rotor, resulting in poor performance predictions. In reality, the lower rotor blades receive either upwash or a small amount of downwash near the blade tip due to the wake contraction. Without the wake contraction, the lower rotor receives excessive downwash from the upper rotor and generates higher torque values than to be expected.

Despite the significant improvements in the coaxial rotor system and the lower rotor figure of merit predictions, the CMTSVT inflow model has a better figure of merit correlation at the upper rotor. The addition of the wake contraction somewhat leads to an underestimated hover efficiency. It should be noted that the wake contraction and decay effects are added to the upper rotor downwash received by the lower rotor. Perhaps, additions of these real-flow effects disturbed the existing interaction balance in the rigid wake formulation and induced some deterioration to the upper rotor figure of merit results. Since the lower rotor operates within the presence and the wake of the upper rotor, some other flow effects might be needed the improve the interaction effects on the upper rotor due to the lower rotor. References 27 and 28 showed that the finite state multirotor inflow models (PPSIM and VPSIM) tend to overestimate the interaction effects of the lower rotor on the upper rotor compared to the viscous vortex particle method predictions. Understanding the cause of this difference between the rigid wake models and high/mid-fidelity models might lead to the identification of new missing real-flow effects.

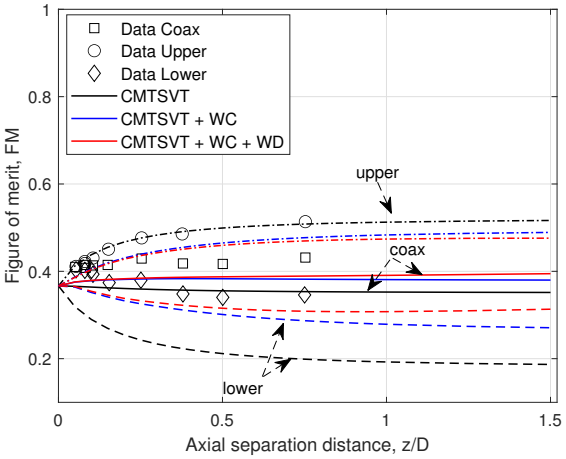

(a) $C_{T_c} = 0.007$

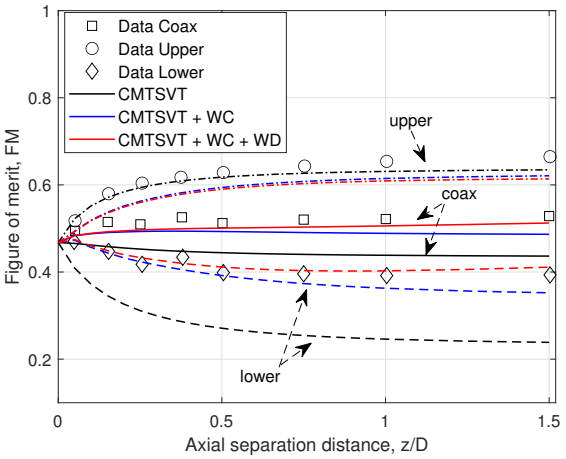

(b) $C_{T_c} = 0.014$

Figure 6: Figure of Merit Predictions at Various Axial Separation Distances ($RPM = 800$).

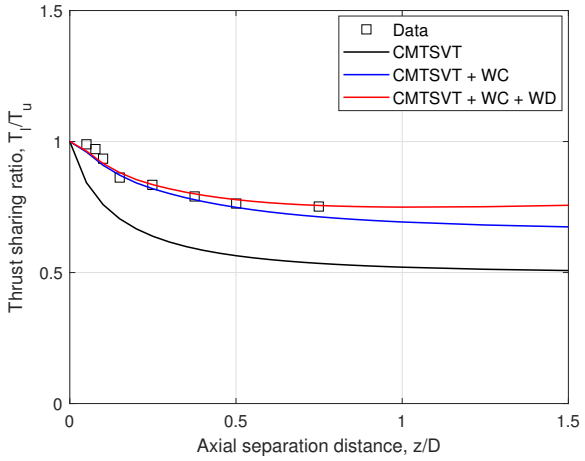

(a) $C_{T_c} = 0.007$

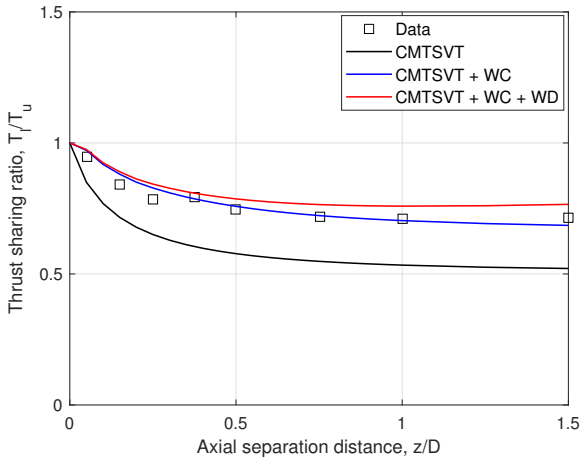

(b) $C_{T_c} = 0.014$

Figure 7: Thrust Sharing Ratio Between the Rotors at Various Axial Separation Distances ($RPM = 800$).

Figure 7 shows the thrust sharing ratio between the lower and upper rotors of the investigated coaxial rotor configurations as a function of vertical separation distance at two different thrust settings. Differences between the low and high thrust settings predictions are most likely due to the selection of simulation parameters such as κ, δ_0, and δ_2. While having a trend similar to the experiment, the CMTSVT inflow model predictions significantly underestimate the lower rotor thrust due to excessive downwash received from the upper rotor. The wake contraction and decay effects make thrust sharing ratio predictions significantly better. The wake decay shows a visible effect for separation distances greater than $0.5D$. Without wake contraction and decay, the thrust sharing ratio settles after the axial separation distance becomes more than one diameter, and the upper rotor produces thrust roughly two times larger than the lower rotor. With the real-flow effect additions, the thrust sharing ratio settles at a shorter distance while predicting a more realistic thrust sharing ratio between the rotors.

Next, the effects of the rotor-rotor interactions on the induced power predictions are studied. The interference loss factor (κ_{int}) describes the necessary increase in the coaxial rotor induced power compared to the case with two rotors in isolation. While κ_{int} designates the overall system loss, rotor-rotor influence loss factors (κ_u & κ_l) provide information on the required increase in the induced power of individual rotors compared to a rotor in isolation at the same thrust condition. The interference and rotor-rotor influence loss factors are calculated using the following equations.

$$\kappa_{int} = \frac{C_{P_{ic}}}{2C_{P_{is}}} \tag{18}$$

$$\kappa_u = \frac{C_{P_{iu}}}{C_{P_{is}}}, \quad \kappa_l = \frac{C_{P_{il}}}{C_{P_{is}}} \tag{19}$$

Figure 8 exhibits the interference loss factor (κ_{int}) predictions at different axial separation distances. The CMTSVT inflow model predicts an increase in the κ_{int} contrary to the decrease in the data and predictions of the CMTSVT inflow model with real-flow effects. The interference inflow received by the lower rotor increases with the separation distance since the wake accelerates and contracts to satisfy continuity. In rigid wake models, induced velocity increases along with the distance. In fact, its magnitude doubles when the flow becomes fully developed. This increase in the induced velocity magnitude is distributed over the entire lower rotor resulting in less efficient (overestimated C_{P_i}) rotor predictions. On the other hand, the introduction of the wake contraction to the CMTSVT inflow model adjusts the interference area accordingly, causing a decrease in the effect brought by the interference inflow. As axial separation distance increases further, the wake decay effect becomes significant. Thus, the interference loss factor continues to decrease with the distance. This trend is expected because vortices should lose all of their strength and completely diffuse with the atmosphere at extreme separation distances. At such extreme distances, all interaction effects will disappear.

Rotor-rotor influence factors of the upper (κ_u) and lower (κ_l) rotors are provided in Fig. 9. At the upper rotor, the CMTSVT inflow model has slightly better agreement with the measurements compared to other cases. As seen, the effect of the lower rotor

on the upper rotor quickly diminishes with the separation distance. In fact, it would be a fair assumption to neglect the lower rotor interaction effect on the upper rotor after the distances longer than the quarter diameter ($z \geq 0.25D$) where κ_u almost reduces to 1. Contrary to κ_u, κ_l increases first and then almost settles when the flow becomes fully developed. The wake contraction has a substantial effect on κ_l at all axial separation distances. Ignoring it leads to highly inefficient lower rotor performance predictions. The addition of the wake decay further improves the correlation at the higher axial separation distances ($z \geq 0.5D$).

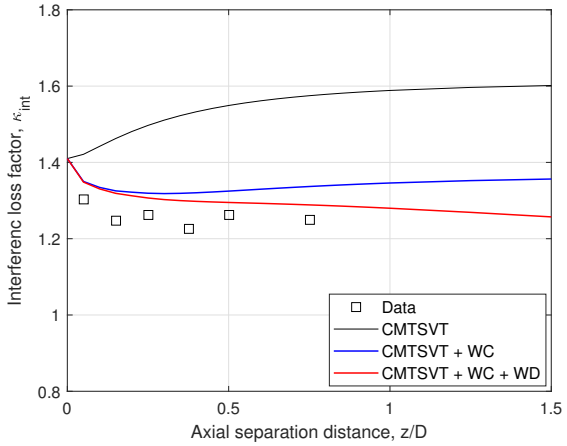

Figure 8: Interference Loss Factor Predictions at Various Axial Separation Distances ($RPM = 800$, $C_{T_c} = 0.014$).

Figures 6–9 show that performance predictions are fairly associated with the wake contraction. In this study, the Landgrebe tip vortex locations [26] are used to determine the wake contraction ratio, which is provided in Fig. 10. As seen, the wake contraction ratio rapidly changes with the axial separation distance and reaches the wake contraction limit (fully developed flow). Typically, the wake geometry changes due to interaction effects. Reference 2 showed that the upper rotor wake contracts more than the rotor in isolation. Perhaps, the usage of a better wake contraction formulation, which can be identified from an experiment or higher-order wake model, might further improve the correlations. Nevertheless, the presented simple wake contraction formulation has already improved the results significantly.

Figures 11 and 12 show the total, self, and interference uniform inflow components as a function of axial separation distance at the upper rotor and lower rotor, respectively. The interference uniform inflow component at the upper rotor quickly weak-

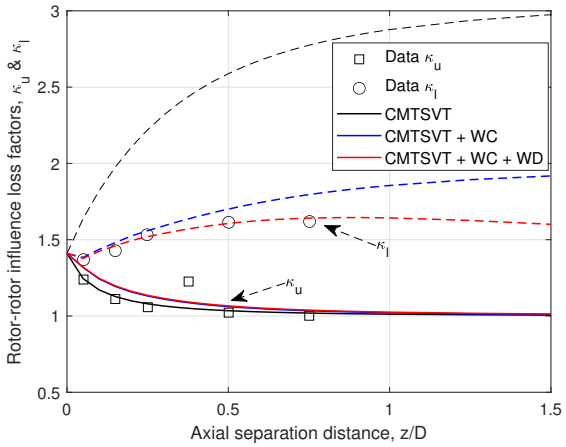

Figure 9: Rotor-Rotor Influence Factors Predictions at Various Axial Separation Distances ($RPM = 800$, $C_{T_c} = 0.014$).

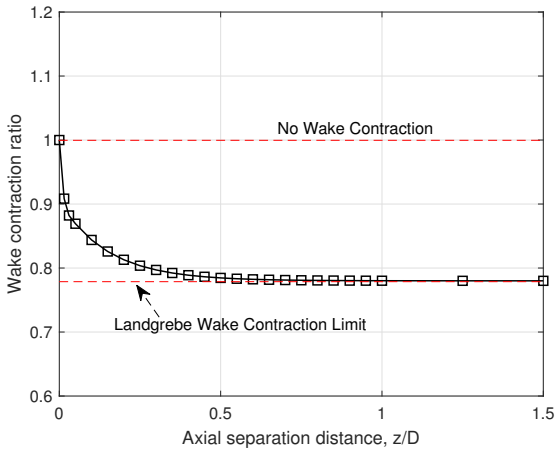

Figure 10: Landgrebe Wake Contraction Ratio versus Axial Separation Distance ($RPM = 800$, $C_{T_c} = 0.014$).

ens with the axial separation distance, and the upper rotor is practically free from interference effects of the lower rotor at distances longer than $0.5D$. At the lower rotor (Fig. 12), the self-induced uniform inflow components of all CMTSVT cases decrease with the axial separation distance as the magnitude of downwash impingement from the upper rotor to the lower rotor increases. In the CMTSVT inflow model with wake contraction and decay, this increase in the downwash magnitude stops at a separation distance of $0.85D$. It then decreases due to substantial wake decay effects. On the other hand, interference inflow predictions of the CMTSVT and CMTSVT+WC increase with the axial separation distance until the flow reaches the fully developed con-

dition. Nevertheless, ignoring the wake contraction effect again leads to high interference inflow predictions on the lower rotor, as shown in Fig. 12.

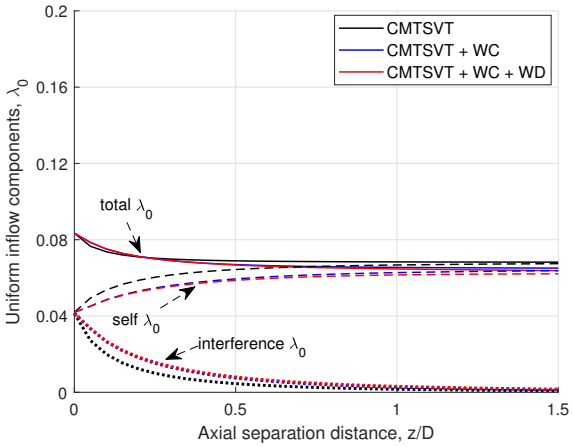

Figure 11: Upper Rotor Total, Self, and Interference Uniform Inflow Components at Various Axial Separation Distances ($RPM = 800$, $C_{T_c} = 0.014$).

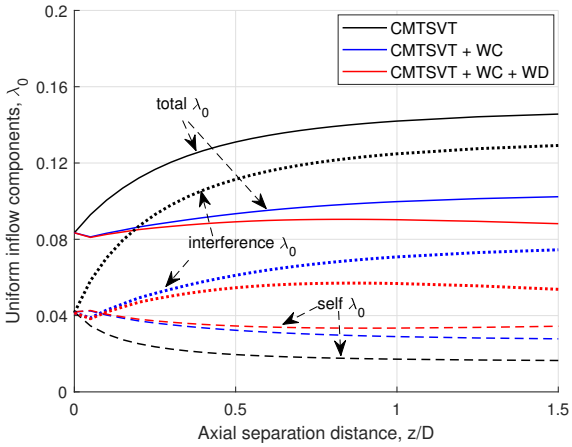

Figure 12: Lower Rotor Total, Self, and Interference Uniform Inflow Components at Various Axial Separation Distances ($RPM = 800$, $C_{T_c} = 0.014$).

The difference between the model with and without wake contraction can be seen in the inflow distribution plots of the lower rotor provided in Fig. 13. When the wake contraction is included, the tip region of the lower rotor operates under a small amount of downwash in contrast to the case without wake contraction. As seen in Fig. 13, the magnitude of the downwash increases with the axial separation distance for both cases. The wake contraction region also becomes larger with the axial separation distance until it settles at 0.78, the theoretical limit of the Landgrebe tip vortex equations.

4. CONCLUSIONS

The wake contraction and decay effects are incorporated into the **c**ombined **m**omentum **t**heory and **s**imple **v**ortex **t**heory (CMTSVT) multirotor inflow model. The original CMTSVT formulation and its updated versions are compared against the wind tunnel measurements to study the effects of loading changes at a fixed axial separation distance and different axial separation distances at fixed loading settings. It has been shown, despite the lack of tuning effort, that the wake contraction and decay additions tremendously improve the predictions of the CMTSVT inflow model, especially for the varying axial separation distance cases. The following conclusions are drawn from this work:

1. The wake contraction effect is significant in hover for coaxial rotor configurations and should be included at moderate and large separation distances.

2. The wake decay effect grows with the separation distance and should be included for separation distances greater than half the rotor diameter.

3. Ignoring the real-flow effects, especially the wake contraction, leads to an overestimation of interaction effects resulting in poorer performance predictions than to be expected at the lower rotor.

4. The incorporation of the wake contraction and wake decay functions slightly degraded the upper rotor predictions despite the significant improvements in the lower rotor and overall coaxial system performance predictions.

5. The interference effect on the upper rotor due to the lower rotor diminishes quickly and can be practically ignored after the separation distances greater than half the rotor diameter.

REFERENCES

[1] Vertical Flight Society, “Press Release: VFS Electric VTOL Directory Hits 600 Concepts,” Fairfax, Virginia, January 2022. Retrieved from https://vtol.org/news/press-release-vfs-electric-vtol-directory-hits-600-concepts.

[2] Kim, H. W., and Brown, R. E., “A Comparison of Coaxial and Conventional Rotor Performance,” *Journal of the American Helicopter Society*, **55**, 012004 (2010), DOI: 10.4050/JAHS.55.012004.

[3] Lakshminarayan, V. K., and Baeder, J. D., "High-Resolution Computational Investigation of Trimmed Coaxial Rotor Aerodynamics in Hover," *Journal of the American Helicopter Society*, **54**, 042008 (2009), DOI: 10.4050/JAHS.54.042008.

[4] Bagai, A., and Leishman, J. G., "Free-Wake Analysis of Tandem, Tilt-Rotor and Coaxial Rotor Configurations," *Journal of the American Helicopter Society*, Vol. 41, (3), July 1996, pp. 196–207, DOI: 10.4050/JAHS.41.196.

[5] Xin, H., Goss, J., and Parkes, C., "Development of a Three State Rotor Interference Model and Application to Coaxial Rotor Inflow Modeling," Proceedings of the American Helicopter Society 5th Decennial Aeromechanics Specialists' Conference, San Francisco, California, January 2014.

[6] Rand, O., and Khromov, V., "Free-Wake Based Dynamic Inflow Model for Hover, Forward and Maneuvering Flight," *Journal of the American Helicopter Society*, **63**, 012008 (2018), DOI: 10.4050/JAHS.63.012008.

[7] Rand, O., and Khromov, V., "Parametric Study of Dynamic Inflow for Single and Coaxial Rotor Systems," *Journal of the American Helicopter Society*, **63**, 042007 (2018), DOI: 10.4050/JAHS.63.042007.

[8] Hersey, S., Celi, R., Juhasz, O., and Tischler, M. B., "Inflow System Identification for Coaxial-Pusher Rotorcraft in Cruising Flight," Proceedings of the 75th Annual Forum of the Vertical Flight Society, Philadelphia, Pennsylvania, May 2019.

[9] Keller, J. D., McKillip, R. M., Wachspress, D. A., Tischler, M. B., and Juhasz, O., "Linearized Inflow and Interference Models from High Fidelity Free Wake Analysis for Modern Rotorcraft Configurations," Proceedings of the 75th Annual Forum of the Vertical Flight Society, Philadelphia, Pennsylvania, May 2019.

[10] Juhasz, O., Xin, H., and Tischler, M. B., "Inflow Based Flight Dynamics Modeling Improvements for the Sikorsky X2 Technology™ Demonstrator," Proceedings of the 76th Annual Forum of the Vertical Flight Society, Virtual, October 2020.

[11] He, C., Gladfelter, M., Chang, C., Tischler, M. B., and Juhasz, O., "VPM Derived State Space Inflow Model for Multi-rotor Air Vehicle Modeling and Simulation," Proceedings of the 75th Annual Forum of the Vertical Flight Society, Philadelphia, Pennsylvania, May 2019.

[12] Kim, J., Sankar, L. N., and Prasad, J. V. R., "Application of a Navier–Stokes Free Wake Hybrid Methodology to the Harrington Coaxial Rotor," Proceedings of the American Helicopter Society Aeromechanics Specialists' Conference on Aeromechanics Design for Vertical Lift, San Francisco, California, January 2016.

[13] Kong, Y.–B., Prasad, J. V. R., Sankar, L. N., and He, C., "Finite State Inflow Flow Model for Coaxial Rotor Configuration," *Journal of the American Helicopter Society*, **65**, 032002 (2020), DOI: 10.4050/JAHS.65.032002.

[14] Guner, F., Prasad, J. V. R., Sankar, L. N., Peters, D. A., and He, C., "Correlation of Finite State Multi-Rotor Dynamic Inflow Models with a High Fidelity Viscous Vortex Particle Method," Proceedings of the 44th European Rotorcraft Forum, Delft, the Netherlands, September 2018.

[15] Guner, F., and Prasad, J. V. R., "Combined Momentum Theory and Simple Vortex Theory Inflow Model for Multirotor Configurations," *Journal of the American Helicopter Society*, **67**, 022007 (2022), DOI: 10.4050/JAHS.67.022007.

[16] Guner, F., Hariani, J., and Prasad, J. V. R., "A Study to Examine Effects of the Inflow Interference on Induced Power Using Combined Momentum and Simple Vortex Theory Inflow Model," Proceedings of the 47th European Rotorcraft Forum, Virtual, September 2021.

[17] Hariani, J., Guner, F., and Prasad, J. V. R., "Evaluation of a Combined Momentum Theory and Simple Vortex Theory (CMTSVT) Inflow Model for UAM Applications," Proceedings of the Vertical Flight Society Aeromechanics for Advanced Vertical Flight Technical Meeting, San Jose, California, January 2022.

[18] Guner, F., "A Multirotor Inflow Model Based on Combined Momentum Theory and Simple Vortex Theory (CMTSVT) for Flight Simulations," Proceedings of the 78th Annual Forum of the Vertical Flight Society, Fort Worth, Texas, May 2022.

[19] Ramasamy, M., "Hover Performance Measurement Toward Understanding Aerodynamic Interference in Coaxial, Tandem, and Tilt Rotors", *Journal of the American Helicopter Society*, **60**, 032005 (2015), DOI: 10.4050/JAHS.60.032005.

[20] Lee, S., and Dassonville, M., "Iterative Blade Element Momentum Theory for Predicting Coaxial Rotor Performance in Hover", *Journal of the American Helicopter Society*, **65**, 042005 (2020), DOI: 10.4050/JAHS.65.042005.

[21] Leishman, J. G., *Principles of Helicopter Aerodynamics*, Cambridge University Press, New York, NY, 2006, Chapter 2.

[22] Johnson, W., *Rotorcraft Aeromechanics*, Cambridge University Press, New York, NY, 2013, Chapters 4 and 5.

[23] Zhao, J., Dynamic Wake Distortion Model for Helicopter Maneuvering Flight, Ph.D. thesis, Georgia Institute of Technology, March 2005.

[24] Heyson, H. H., "Equations for the Induced Velocities Near a Lifting Rotor with Nonuniform Azimuthwise Vorticity Distribution," NASA TN D-394, August 1960.

[25] He, C., Xin, H., and Bhagwat M., "Advanced Rotor Wake Interference Modeling for Multiple Aircraft Shipboard Landing Simulation," Proceedings of the 59th Annual Forum of the American Helicopter Society, Baltimore, Maryland, June 2004.

[26] Landgrebe, A. J., "An Analytical and Experimental Investigation of Helicopter Rotor Hover Performance and Wake Geometry Characteristics," USAAMRDL Technical Report 71–24, Eustis Directorate U. S. Army Air Mobility Research and Development Laboratory, Fort Eustis, Virginia, June 1971.

[27] Kong, Y.–B., Prasad, J. V. R., and He, C., "Finite State Coaxial Rotor Inflow Model Enhancements Using VVPM-Extracted Influence Coefficients", **65**, 022008 (2020), DOI: 10.4050/JAHS.65.022008.

[28] Guner, F., Prasad, J. V. R., He, C., and Peters, D. A., "Fidelity Enhancement of a Multirotor Dynamic Inflow Model via System Identification," *Journal of the American Helicopter Society*, **67**, 022009 (2022), DOI: 10.4050/JAHS.67.022009.

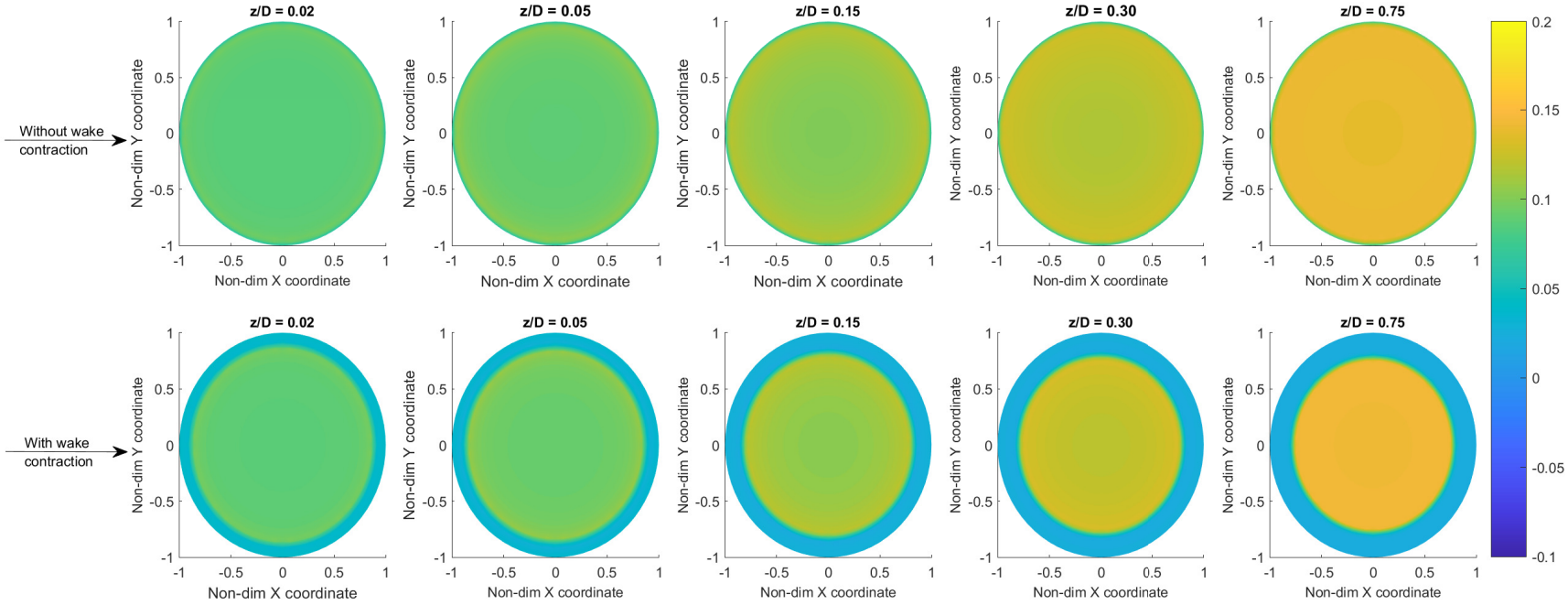

Figure 13: The CMTSVT Lower Rotor Inflow Distribution Predictions at Various Axial Separation Distances ($RPM = 800$, $C_{T_c} = 0.014$).